



Alexandria University  
**Alexandria Engineering Journal**

[www.elsevier.com/locate/aej](http://www.elsevier.com/locate/aej)  
[www.sciencedirect.com](http://www.sciencedirect.com)



## ORIGINAL ARTICLE

# Feasibility study of performing experimental modal analysis with oblique impact testing using various oblique impact directions

Shin Yee Khoo <sup>a,\*</sup>, Yee Cheng Lian <sup>a</sup>, Zhi Chao Ong <sup>a</sup>, Zubaidah Ismail <sup>b</sup>, Siamak Noroozi <sup>c</sup>

<sup>a</sup> Department of Mechanical Engineering, Engineering Faculty, University of Malaya, 50603 Kuala Lumpur, Malaysia

<sup>b</sup> Department of Civil Engineering, Engineering Faculty, University of Malaya, 50603 Kuala Lumpur, Malaysia

<sup>c</sup> School of Design, Engineering & Computing, Bournemouth University, Poole, Dorset BH12 5BB, UK

Received 19 September 2019; accepted 9 January 2020

## KEYWORDS

Dynamic characteristic;  
 Frequency response function synthesis method;  
 Modal testing;  
 Oblique angle;  
 Oblique impact;  
 Tri-axial normal impact testing

**Abstract** Oblique impact excitation has been introduced in Experimental Modal Analysis (EMA), with the great advantage of reducing the conventional EMA's testing time by a factor of three. One major constraint of this technique is the investigation of the effect of various oblique impact directions towards its accuracy in determining the structural dynamic characteristic. This feasibility study is difficult to be achieved in practice, as it involves a lengthy amount of experimental works using various oblique impact directions. To solve this problem, a mathematical model has been developed to synthesize the FRF due to oblique impact (i.e. oblique FRF) in this study. The synthesized oblique FRFs show great agreement with the measured oblique FRFs in various oblique impact directions, which validate the reliability of the usage of the proposed synthesis method. The performance of the oblique impact testings using various impact angles is investigated. The results show that the oblique impact testing has a high success rate to extract directional modes in many impact directions, however wrong selection of the impact direction will lead to mode estimation failure. Good selection of impact direction based on force and modal strengths are demonstrated to ensure an accurate estimation of the structural dynamic characteristics.

© 2020 Faculty of Engineering, Alexandria University. Production and hosting by Elsevier B.V. This is an open access article under the CC BY-NC-ND license (<http://creativecommons.org/licenses/by-nc-nd/4.0/>).

## 1. Introduction

Experimental modal analysis (EMA) is well established since decades ago to obtain accurate dynamic characteristics of a structure, such as natural frequency, modal damping ratio and mode shape. In general, EMA involves the measurement of the input force, and the output response of the system [1]. Its applications involved crack detection of cantilever beam

\* Corresponding author.

E-mail addresses: [khooshinyee@um.edu.my](mailto:khooshinyee@um.edu.my), [mikeson.khoo@yahoo.com](mailto:mikeson.khoo@yahoo.com) (S.Y. Khoo).

Peer review under responsibility of Faculty of Engineering, Alexandria University.

<https://doi.org/10.1016/j.aej.2020.01.014>

1110-0168 © 2020 Faculty of Engineering, Alexandria University. Production and hosting by Elsevier B.V.

This is an open access article under the CC BY-NC-ND license (<http://creativecommons.org/licenses/by-nc-nd/4.0/>).

[2], damage detection of flexural structural systems [3], modal analysis on tire [4] and etc. The broadband frequency characteristic of the force is desired for shorter testing time, therefore impact force from an impactor or random excitation from a shaker is commonly used in EMA. Compared to shaker testing, EMA with impact testing does not introduce any inertia loading effect on the structure, plus it has less demanding criteria in terms of instrumentation and test set-up complexity. Thus, it will be used in this study. With the transfer function strategy, the system's dynamic behavior can be expressed in the form of frequency response function (FRF) in frequency domain involving the response and force data. Any unaccounted force must be avoided while conducting EMA as it will affect the FRF quality, so EMA must be conducted during the non-operating condition. Once the complete FRF data is ready, the desired modal parameters of the structure can be obtained through the curve-fitting algorithm.

To conduct a successful EMA, the selection of the reference degree of freedom (DOF) requires comprehensive consideration. First of all, all modes in the frequency range of interest must be excitable at the selected reference DOF, i.e. none of the modes of interest can have a node at the reference DOF [5]. Secondly, the reference DOF can be selected as fixed force DOF or fixed response DOF, as long as a complete row/column of the FRF matrix can be obtained. This can be done by using the roving accelerometer or roving force approaches. As a rule of thumbs, the mass loading effect must be taken into consideration when the roving accelerometer approach is chosen. Corrective action must be taken if there is a peak shift in FRF, especially when the attached transducer's mass exceeds 10% of the test object [6]. Furthermore, the roving force approach is free of the mass loading effect and FRF's peak shift problem. Roving the impactor between measurement points (i.e. roving force approach) is far much easier than remounting the response transducer (i.e. roving response approach) in many cases, which results in a more consistent measurement as well as the reduction in testing time and effort [7]. However, the roving force approach is only applicable to simple structure, which consists of the predominantly unidirectional motion of the vibration modes. For a 3D complex structure, which consists of the predominantly multidirectional motion of the vibration modes, the roving force approach always provides an incomplete row of the FRF matrix due to the difficulty of applying force excitation in three orthogonal directions at all measurement locations. In case it may not be physically possible to excite the test object in such a manner, the roving accelerometer approach is more favourable to tackle the vibration problem of a 3D complex structure.

The third consideration would be the sufficient number of reference DOF for EMA. Mono-reference or single reference technique is firstly introduced which involves the measurement of a single complete column/row of the FRF matrix. Theoretically, it is assumed that this non-nodal reference DOF is sufficient to determine all the modes of interest. However, it is crucial to understand that the single reference technique is only able to reveal the vibration modes in a predominantly unidirectional motion, from a practical standpoint. If either direction of excitation is chosen, the other mode shape by the other excitation direction apparently would not appear [8]. Thus, multi-reference technique is strongly recommended because it allows the adequate description of all the modes from the com-

ination of references which gives the best possible chance to adequately determine all of the modes of the system [9,10]. This is particularly useful when repeated mode or closely coupled mode exists (i.e. two or more modes appear in identical or close natural frequency which cannot be found using the single reference technique). These intractable modes are frequently found in symmetric structure or sometimes the structure of arbitrary geometries that exhibit repeated roots [11,12] or dynamically complex structure with 3D mode shapes comprised of several directional modes in various orthogonal planes [9,13]. As demonstrated by previous researchers [9,11,13–15], the first case can be successfully tackled by selecting two or more reference DOFs in various measurement locations. For example, the roving force approach can be applied while fixing the accelerometers at multiple locations, to find the dynamic characteristics of the structure with repeated roots. The selection of useful reference locations is important for the success of the testing. A priori knowledge of the examined similar structure can be used for the choice of reference DOFs. Else, a 'short-gun' approach (i.e. selecting a large number of randomly chosen references) would be useful, though less efficiently for an unknown structure [9].

Moreover, the latter case (i.e. dynamically complex structure) is more troublesome to be solved as it requires reference force DOF to be selected in the three principal directions, i.e. axial, horizontal and vertical axes of the structure, to reveal several directional modes in various orthogonal planes. The friendly roving force approach is no longer suitable to solve the latter case due to the physical constraint of the test object that limits the obtainable measurements. Hence, the roving response approach must be applied to solve this problem, while fixing the impact force at three principal directions of the selected non-nodal point [16]. This tri-axial normal impact testing strategy is well-established in the state of art and it is often used as benchmark for any newly developed modal testing approach. Previous works [17,18] highlighted that this strategy requires extremely long testing time due to the redundant procedure of impactor as well as the sensor remounting procedure. This is unfavorable to numerous industries especially the petrochemical industry where the cost of downtime and unscheduled shutdown can be as high as USD 100,000 per day [19]. Moreover, impacting in three orthogonal directions aligned with the defined global coordinate system may not be possible at the non-nodal point of some structures due to the physical constraint in the practical scenario [20]. The inability to properly excite the system will eventually cause inconsistent or failure in obtaining the modal data.

To reduce the EMA's testing time, the idea of oblique force reference DOF has emerged. In fact, a single oblique force can excite the structures in all principal directions, hence ensures the participation of all modes in various principal directions [12,17]. Døssing [5] claimed that the oblique reference DOF poses the modal decoupling advantage for closely-spaced modes with predominantly orthogonal motion if the right combination of position and direction can be selected on this reference. He highlighted that the selected oblique DOF must ensure a balance of modal strength (equal magnitude in frequency response) and excite all modes of interest. The study developed a special fixture that allowed the oblique input force acting at 45° relative to the attached surface. A similar set-up was followed by Warren et al. [21,22] who conducted the oblique impact and shaker testings on a base-upright (BU)

structure. The BU structure exhibited predominantly mode shapes in the axial and vertical directions in the upright and base parts respectively. However, the testing only focused on the upright part which simplified the problem to axial directional mode. Besides, Avitabile [23] suggested that the reference DOF can be selected at any oblique angle as long as it can excite all the modes of interest, while Baqersad [24] demonstrated the mode shape scaling procedure by using the oblique reference driving point FRF, without the need to identify the orientation of the input force. Moreover, the oblique angle information is neglected by most of the researchers where it can be seen from previous studies that did not report the oblique angle information for the oblique testing in various types of structures, such as three-bladed wind turbine [24,25], fuselage panel [26], stripline structure [27], tire [28], vehicle body [20,29] and human tibia [30]. However, it is still not sure the selected reference DOF at various oblique angles can have a balance modal strength for successful modal decoupling.

To date, the effectiveness of the selected oblique reference DOF in various directions was not examined in the previous literature. In fact, a suitable oblique angle is crucial to determine the success of oblique testing and the wrong selection of it might lead to failure in revealing the intractable modes, without the user noticed it. Thus, it is vital to understand the effect of various oblique angles on the accuracy of the estimated modal parameters so that the users can understand the effectiveness of selecting the suitable oblique angle in their testing. To achieve this, a substantial amount of oblique impact data must be acquired to study intensively the feasibility of various oblique excitation directions for accurate modal parameter estimation. This requirement has certainly increased the difficulty in evaluation, as there are many possibilities of oblique impact angles, which is very time consuming and impractical in carrying out experimentally. In this paper, an alternative approach to estimate the oblique FRFs at various oblique angles is developed, which involves only the measurement of the normal FRFs at the 3 orthogonal directions. Thus, the experiment testing time can be reduced tremendously and it makes the feasibility study of the 'oblique angle effect' possible and achievable in this study.

## 2. Material and methods

### 2.1. Experimental modal analysis with multi-reference normal impact testing

The test structure of this research is a T-shaped rig with 19 measurement points, as shown in Fig. 1. Multi-reference EMA with tri-axial normal impact testing is performed to measure the dynamic properties of the structure and it will be used as the benchmark against the result of the oblique reference EMA. In this study, a 4-channel data acquisition system equipped with an instrumented impact hammer and a tri-axial accelerometer is used for EMA. The block size and sampling rate of the FRF measurement are set at 4096 samples and 2048 Hz respectively. This setting gives a time resolution of 0.0004882 s and frequency resolution of 0.5 Hz, which are sufficient to measure both impact force and response signals satisfactorily.

The roving accelerometer approach is implemented for the testing. The structure is first excited in the axial direction

(x-axis) at Point #1 using an instrumented impact hammer, while the tri-axial accelerometer is roved from Points #1 to #19 for 19 measurements. The response and force data are collected for 5 averages per measurement point, to reduce the measurement noise. This process is repeated by applying the normal forces in the horizontal direction (y-axis) and vertical direction (z-axis) respectively. In this way, the multi-reference force DOFs selected in the three principal directions will produce 3 complete columns of the FRF matrix as shown in Eq. (1).

$$\mathbf{H}_{xyz}(\omega) = \begin{bmatrix} H_{1x:1x} & H_{1x:1y} & H_{1x:1z} \\ H_{1y:1x} & H_{1y:1y} & H_{1y:1z} \\ H_{1z:1x} & H_{1z:1y} & H_{1z:1z} \\ \vdots & \vdots & \vdots \\ H_{19x:1x} & H_{19x:1y} & H_{19x:1z} \\ H_{19y:1x} & H_{19y:1y} & H_{19y:1z} \\ H_{19z:1x} & H_{19z:1y} & H_{19z:1z} \end{bmatrix} \quad (1)$$

where  $\mathbf{H}_{xyz}$  is the three-column FRF matrix measured from the multi-reference EMA in the frequency domain ( $\omega$ ).  $\bullet_{xyz}$  indicates the multi-reference force DOFs at x-, y- and z-axes respectively. Each element in the FRF matrix is in the form of  $H_{ni:mj}$ , where  $n$  and  $m$  are the position DOFs, while  $i$  and  $j$  are the direction DOFs, for the output response and input force respectively. Considering the transient characteristics of the impact force and response signals, the FRF is obtained through the following equation as follows ISO 7626-1:2011 (E) [31].

$$H_{ni:mj}(\omega) = \frac{\ddot{X}_{ni}(\omega)}{F_{mj}(\omega)} \quad (2)$$

where  $F_{mj}(\omega)$  is the impact force in the frequency domain, which is acting at the  $m$ -position and  $j$ -direction, while  $\ddot{X}_{ni}(\omega)$  is the impact-induced response in the frequency domain, which is acquired from the  $n$ -position and  $i$ -direction of the test rig. In general,  $ni$  and  $mj$  are the response and force DOFs respectively.

The overlaid of the multi-reference FRFs obtained from the tri-axial normal impact testing is shown in Fig. 2. The scope of the study is limited to the first 3 natural frequencies of the structure according to the operating environment. From Fig. 2, it is observed that there are 3 global peaks within 25 Hz indicating the 3 vibration modes in this frequency range.

To obtain the actual number of modes and pole location, multi-reference mode indicator and modal participation factor (also known as relative mode shape strength) are computed by using ME'scope® software. In terms of the multi-reference mode indicator, complex mode indicator function (CMIF) is used because it can detect repeated roots and closely coupled modes from multi-reference data. CMIF involves the singular value decomposition (SVD) to decompose the multi-reference FRF matrix into a product of three matrixes, as shown in Eq. (3).

$$\mathbf{H}_{xyz}(\omega) = \mathbf{U}(\omega)\mathbf{\Sigma}(\omega)\mathbf{V}^H(\omega) \quad (3)$$

where  $\mathbf{U}(\omega)$  and  $\mathbf{V}(\omega)$  are the left and right singular matrices and they have orthogonal columns.  $\mathbf{\Sigma}(\omega)$  is the diagonal matrix of singular value.  $\bullet^H$  denotes the Hermitian transpose.

CMIF is equal to the square of the singular value (i.e.  $\Sigma^2(\omega)$ ) while the right matrix is related to the modal

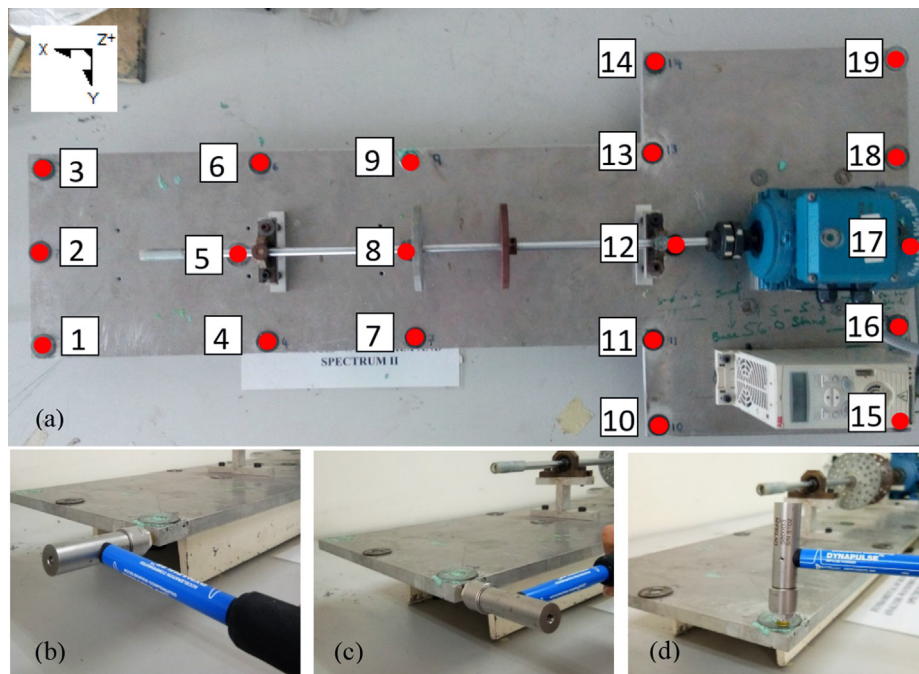


**Fig. 1** (a) T-shaped test rig and the normal impact in (b) x-, (c) y-, and (d) z- directions.

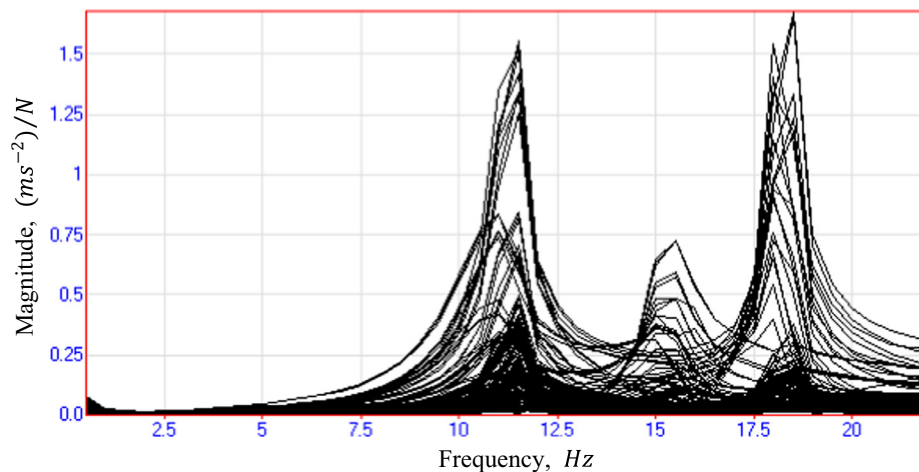


**Fig. 2** Multi-reference FRFs obtained from EMA with tri-axial normal impact testing.

participation factor. The detail of the CMIF and modal participation factor can be found in Refs. [15,32,33]. The CMIF result of the multi-reference FRFs is shown in Fig. 3 and Table 1. There are three CMIF curves obtained from three normal forces references acting in the x-, y- and z- directions respectively. Fig. 3 shows that the primary CMIF curve is due to z-excitation reference. It consists of 3 peaks indicating the presence of vibration modes. The secondary CMIF curve of y-excitation reference shows there is a peak closely spaced with the first mode of the primary curve indicating the closely coupled mode. The tertiary CMIF curve of x-excitation has a negligible singular value compared to the other two curves, hence it has no repeated/ coupled mode within this frequency range. In total, there are 4 vibration modes successfully identified by using the CMIF curves as shown in Table 1.

Next, the modal participation factor of the identified vibration modes is given in Table 1. In fact, ME'scope® computes the modal participation factor in the form of relative mode shape strength which ranges from 0 (i.e. meaning that mode has a weak contribution and most likely not present at the reference) to 10 (i.e. meaning that mode has a strong contribution and it is strongly present at the reference), as demonstrated in references [34,35]. The strongest represented reference DOFs for each mode are labelled with '\*' in Table 1. They will be selected for further mode shape extraction using multi-reference polynomial curve fitting methods in ME'scope®. Modal assurance criterion (MAC) between the generated mode shapes will be obtained. In specific, the comparison between mode shapes to itself is called 'Auto-MAC' in this study. Note that Auto-MAC greater than 0.9 is considered as excellent

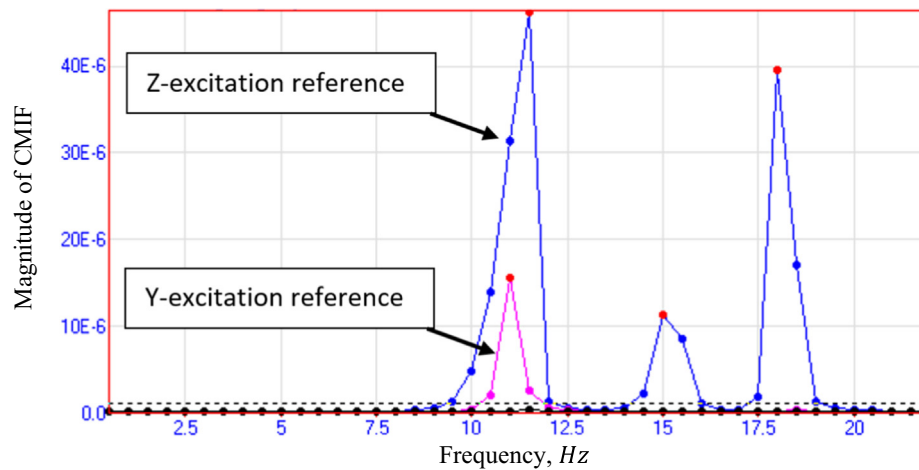


Fig. 3 Peak count window by CMIF.

**Table 1** Relative mode shape strength for impact references in 3 principal directions and the Auto-MAC of the obtained mode shapes.

Mode Indicator Function	Frequency(Hz)	Relative Shape Strength of the Corresponding Reference DOF			Auto-MAC Between Modes to Itself			
		1x	1y	1z	11.33	11.37	15.23	18.24
(i) CMIF	11.33	1.1	1.5*	1.2	1.00	0.41	0.01	0.03
	11.37	0.1	0.5	2.6*	0.41	1.00	0.02	0.04
	15.23	0.0	10.0*	0.0	0.01	0.02	1.00	0.03
	18.24	0.0	0.2	9.7*	0.03	0.04	0.03	1.00
(ii) Modal Peaks Function		1x	1y	1z	11.29	11.35	15.23	18.24
	11.29	0.0	3.5*	0.0	1.00	0.09	0.05	0.02
	11.35	0.0	0.0	10.0*	0.09	1.00	0.01	0.03
	15.23	0.0	9.0*	0.0	0.05	0.01	1.00	0.03
	18.24	0.0	0.0	8.6*	0.02	0.03	0.03	1.00

similarity in terms of mode shapes between the examined modes, while Auto-MAC close to 0 indicates two different mode shapes. The Auto-MAC matrix of the obtained mode shapes is shown in Table 1. The off-diagonal values of 0.41 on the Auto-MAC matrix is obtained, which indicates there is some degree of similarity between the first two modes. This shows that the applied curve-fitting algorithms do not properly extract the mode shapes for the first two modes as each mode shape should be linearly independent between each other.

By trying the other available algorithms in the ME'scope®, modal peaks function [36] and multi-reference polynomial curve fitting method provide the best result in this study. The relative mode shape strength for the first two modes are enhanced by using this curve fitting method. Table 1 shows that the mode shape by y-excitation reference has the highest relative shape strength at 11.29 Hz, while at 11.35 Hz, the mode shape by z-excitation reference has the highest relative shape strength. Hence, Mode #1 contains two closely coupled modes that only can be revealed well by y-excitation and z-excitation references respectively. The remaining Mode #2 and Mode #3 at 15.23 Hz and 18.24 Hz have the highest relative shape strengths at y-excitation and z-excitation references respectively. Next, the selected references with the highest relative shape strength (i.e. with "\*" label) will proceed with the

curve fitting of mode shape. The Auto-MAC matrix of the mode shapes obtained from the modal peaks function and multi-reference polynomial curve fitting method is shown in Table 1. All off-diagonal values are approximately zero indicates that the mode shapes are linearly independent to each other among the four modes. So, the modal parameters are extracted properly using the modal peaks function and multi-reference polynomial curve fitting methods. In this study, the dynamic characteristics obtained at 11.29 Hz, 11.35 Hz, 15.23 Hz and 18.24 Hz will be denoted as 'Mode #1 by y-excitation', 'Mode #1 by z-excitation', 'Mode #2 by y-excitation' and 'Mode #3 by z-excitation' respectively and it will be used as the benchmark results.

## 2.2. Experimental modal analysis with oblique impact testing

In this study, the performance of the oblique impact testing by using various impact angles will be investigated. The experimental set-up for the oblique impact testing is similar to the previous experimental setting, except that the tri-axial force reference DOFs are simplified to an oblique impact direction. Fig. 4 shows the oblique impact force acting at Point #1, where the oblique direction can be varied to the x-, y- and z-axes in terms of angles  $\alpha$ ,  $\beta$  and  $\gamma$  respectively.

The feasibility study of the oblique angle effect in EMA is extremely difficult to achieve in the actual scenario as it requires unreasonable time and effort to achieve that. This study provided an alternative solution to synthesize the oblique FRF due to various oblique impact directions, instead of completing the tough procedure. The alternative method involves the normal FRF data obtained from the tri-axial normal impact testing, as well as the validation procedure of the proposed synthesis method. The data needed for the first case can be prepared according to section 2.1, while the latter case will be conducted by comparing the synthesized modal parameter results with the experimental data. For the validation purpose, 10 sets of oblique impact testings are conducted experimentally by using different oblique angles as shown in Table 2.

The experimental oblique FRFs matrix,  $\mathbf{H}_{ob}(\omega)$  can be measured following Eq. (2) to generate Eq. (5).

$$\mathbf{H}_{ob}(\omega) = \begin{bmatrix} H_{1x:1ob,\varnothing_1} & H_{1x:1ob,\varnothing_2} & \dots & H_{1x:1ob,\varnothing_{10}} \\ H_{1y:1ob,\varnothing_1} & H_{1y:1ob,\varnothing_2} & \dots & H_{1y:1ob,\varnothing_{10}} \\ H_{1z:1ob,\varnothing_1} & H_{1z:1ob,\varnothing_2} & \dots & H_{1z:1ob,\varnothing_{10}} \\ \vdots & \vdots & \dots & \vdots \\ H_{19x:1ob,\varnothing_1} & H_{19x:1ob,\varnothing_2} & \dots & H_{19x:1ob,\varnothing_{10}} \\ H_{19y:1ob,\varnothing_1} & H_{19y:1ob,\varnothing_2} & \dots & H_{19y:1ob,\varnothing_{10}} \\ H_{19z:1ob,\varnothing_1} & H_{19z:1ob,\varnothing_2} & \dots & H_{19z:1ob,\varnothing_{10}} \end{bmatrix} \quad (5)$$

where  $\bullet_{ob,\varnothing_1}, \bullet_{ob,\varnothing_2}, \dots, \bullet_{ob,\varnothing_{10}}$  are the oblique directions at the selected oblique angles of set number #1 – #10 for 10 sets of experimental oblique impact testings according to Table 2.

The synthesized oblique FRF,  $\tilde{H}_{ni:mob,\varnothing}$  can be established using Eq. (6).

$$\tilde{H}_{ni:mob,\varnothing} = \cos \alpha (H_{ni:m_x}) + \cos \beta (H_{ni:m_y}) + \cos \gamma (H_{ni:m_z}) \quad (6)$$

where  $H_{ni:m_x}$ ,  $H_{ni:m_y}$ , and  $H_{ni:m_z}$  are the elements in three-column FRF matrix,  $\mathbf{H}_{xyz}(\omega)$  measured from the tri-axial normal impact testing according to Eq. (1). The unit vector of the oblique impact direction can be quantified by the cosine angles, i.e. arbitrary oblique direction,  $\bullet_{ob,\varnothing} = \{\cos \alpha, \cos \beta, \cos \gamma\}$ . Eq. (6) shows that oblique FRF in any arbitrary oblique directions can be synthesized if the oblique direction and the normal FRFs in three principal directions can be provided. To check the validity of Eq. (6), 10 sets of synthesized oblique impact testings are generated

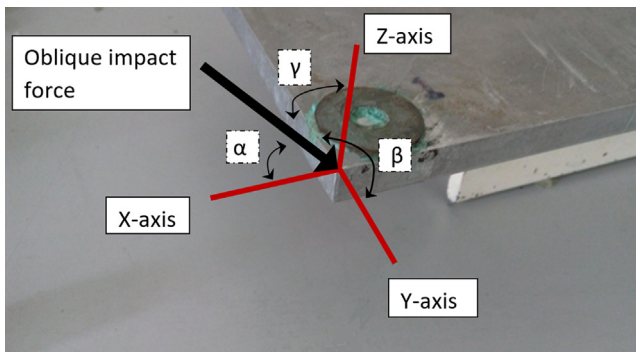


Fig. 4 Illustration of oblique impact force in EMA.

using the oblique impact angles given in Table 2. Hence, the correlation,  $Corr$  between both measured and synthesized mean oblique FRFs are calculated using Eq. (7).

$$Corr = \frac{\left| \sum_{r=0}^{BS-1} \left( H_{ob,\varnothing}^r \tilde{H}_{ob,\varnothing}^{r*} \right) \right|^2}{\left( \sum_{r=0}^{BS-1} \left( H_{ob,\varnothing}^r H_{ob,\varnothing}^{r*} \right) \right) \left( \sum_{r=0}^{BS-1} \left( \tilde{H}_{ob,\varnothing}^r \tilde{H}_{ob,\varnothing}^{r*} \right) \right)} \quad (7)$$

where  $H_{ob,\varnothing}^r$  and  $\tilde{H}_{ob,\varnothing}^r$  are the  $r^{th}$  samples of the mean oblique FRF in a particular oblique direction for both experimental and synthesized data respectively.  $\bullet^*$  is the complex conjugate function. Block size,  $BS$  is the total number of collected samples per block. Note that the correlation value that greater than 0.9 indicates an excellent agreement between the measured and synthesized oblique FRFs. The correlation results for each angle set are shown in Table 2. The range is between (0.927 – 0.994). It shows that the synthesized FRFs are very similar to the measured FRFs, indicating the practicability of the oblique FRF synthesis method to be used in the feasibility analysis next.

To further examine the performance of the synthesized oblique FRF in modal parameter estimation, the dynamic characteristics extracted from synthesized oblique FRF are compared with the results from experimental oblique FRFs. Tables 3–5 shows the comparison between the natural frequency, modal damping ratio and mode shape obtained from experimental and synthesized oblique FRFs respectively. Table 3 shows that the obtained natural frequency from the synthesized oblique FRF has high accuracy, where percentage errors of less than 0.80%, 1.06%, and 0.49% are obtained from Modes #1 to #3 respectively. Table 4 shows that the obtained modal damping ratio is satisfactory as it has maximum absolute errors about 0.63%, 1.05%, and 0.07% for the three examined modes. Next, the MAC is used to identify the similarities between two mode shapes obtained from synthesized and measured FRFs. Note that MAC greater than 0.9 is considered as excellent similarity in term mode shape. Mode shape comparison in Table 5 shows that the synthesized oblique FRFs produce very similar mode shapes as the measured results, where Modes #1, #2 and #3 have MAC values within (0.941–0.988), (0.932–0.983) and (0.960–0.983) respectively. To a great degree, the synthesized oblique FRFs demonstrate great performance in terms of modal parameter estimation and FRF synthesis, as compare with the experimental oblique FRFs. Hence it is validated that the proposed oblique FRF synthesis method is capable to synthesize reliable oblique FRF with great accuracy for further analysis.

For the feasibility study of oblique impact testings using various oblique impact directions, a total of 115 impact directions including 3 normal directions are selected and marked as ‘o’ in Fig. 5. Each impact is knocked towards the measurement position labelled ‘o’ of the structure, which is illustrated at the position (0, 0, 0) in Fig. 5 and it represents the Point #1 of the real structure as shown in Figs. 1(a) and 4. Note that the investigated impact directions are limited to one octant of the spherical space, as it is assumed that oblique excitations at other octants would produce a redundant result. By using the selected directions, 115 sets of synthesized oblique FRFs are obtained as follows Eq. (6). The effectiveness of the oblique angle effect in extracting the modal parameter will be examined next by benchmarking to the conventional

**Table 2** The selected oblique impact direction for experimental oblique impact testing and the FRF correlation result.

Set No.	Angle to x-axis ( $\alpha$ ), °	Angle to y-axis ( $\beta$ ), °	Angle to z-axis ( $\gamma$ ), °	Correlation between Synthesized and Experimental Oblique FRFs
1	46.92	46.92	75.00	0.942
2	52.24	52.24	60.00	0.927
3	60.00	60.00	45.00	0.975
4	69.30	69.30	30.00	0.989
5	79.45	79.45	15.00	0.994
6	79.45	46.92	45.00	0.975
7	69.30	52.24	45.00	0.972
8	52.24	69.30	45.00	0.963
9	46.92	79.45	45.00	0.944
10	54.74	54.74	54.74	0.944

**Table 3** Natural frequency comparison between experimental oblique FRF (Exp) and synthesized oblique FRF (Syn).

Set No.	Natural Frequency								
	Mode #1			Mode #2			Mode #3		
	Exp, Hz	Syn, Hz	Percent Error , %	Exp, Hz	Syn, Hz	Percent Error , %	Exp, Hz	Syn, Hz	Percent Error , %
1	11.29	11.20	0.80	15.19	15.22	0.20	18.34	18.25	0.49
2	11.26	11.19	0.62	15.15	15.23	0.53	18.31	18.25	0.33
3	11.29	11.27	0.18	15.12	15.23	0.73	18.29	18.24	0.27
4	11.29	11.30	0.09	15.07	15.23	1.06	18.26	18.24	0.11
5	11.31	11.34	0.27	N/A	N/A	N/A	18.25	18.24	0.05
6	11.28	11.26	0.18	15.12	15.23	0.73	18.29	18.25	0.22
7	11.30	11.26	0.35	15.14	15.23	0.59	18.29	18.25	0.22
8	11.36	11.29	0.62	15.17	15.23	0.40	18.29	18.24	0.27
9	11.39	11.32	0.61	N/A	N/A	N/A	18.28	18.24	0.22
10	11.25	11.25	0.00	15.36	15.23	0.85	18.26	18.24	0.11

**Table 4** Modal damping ratio comparison between experimental oblique FRF (Exp) and synthesized oblique FRF (Syn).

Set No.	Modal Damping Ratio								
	Mode #1			Mode #2			Mode #3		
	Exp, %	Syn, %	Absolute Error , %	Exp, %	Syn, %	Absolute Error , %	Exp, %	Syn, %	Absolute Error , %
1	3.38	3.58	0.20	2.81	3.77	0.96	1.16	1.14	0.02
2	3.59	2.96	0.63	2.90	3.77	0.87	1.17	1.15	0.02
3	3.01	2.72	0.29	2.96	3.77	0.81	1.21	1.16	0.05
4	2.81	2.60	0.21	2.92	3.77	0.85	1.22	1.16	0.06
5	2.61	2.55	0.06	N/A	N/A	N/A	1.21	1.16	0.05
6	3.19	2.83	0.36	2.75	3.79	1.04	1.24	1.17	0.07
7	3.09	2.79	0.30	2.73	3.78	1.05	1.22	1.17	0.05
8	2.77	2.61	0.16	2.75	3.74	0.99	1.21	1.15	0.06
9	2.69	2.47	0.22	N/A	N/A	N/A	1.21	1.14	0.07
10	2.96	2.79	0.17	3.96	3.77	0.19	1.10	1.15	0.05

multi-reference EMA result. 2D oblique impacts that excite xy-, yz- and xz- planes are labelled as 'Line #1', 'Line #2', and 'Line #3' respectively. 3D oblique angles that excite xyz-plane are labelled as 'Line #4', 'Line #5', and Line #6'. These impact directions are selected so that it can be used to study the oblique force effect with changing contribution of x-, y- and z- excitations respectively.

### 3. Result and discussion

The ultimate objective of EMA is to determine accurate modal parameters such as natural frequency, modal damping ratio, and mode shape. To examine the effectiveness of using various oblique impact directions in the oblique impact testing, the

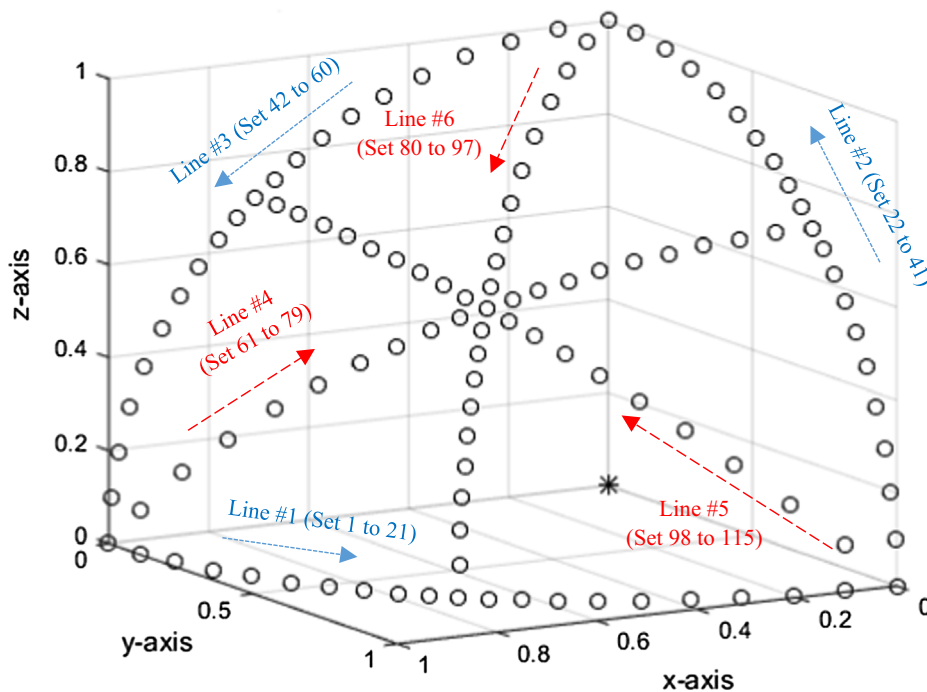
**Table 5** MAC comparison between experimental and synthesized oblique FRFs.

Set No.	MAC		
	Mode #1	Mode #2	Mode #3
1	0.971	0.979	0.965
2	0.941	0.979	0.960
3	0.979	0.971	0.969
4	0.984	0.932	0.976
5	0.988	N/A	0.963
6	0.982	0.983	0.964
7	0.980	0.983	0.976
8	0.974	0.958	0.977
9	0.979	N/A	0.981
10	0.964	0.976	0.983

extracted modal parameters from the synthesized oblique FRFs using various oblique angles will be compared with the result of the well-established multi-reference EMA, i.e. tri-axial normal impact testing. Fig. 6 shows the natural frequencies result obtained from the oblique reference EMA (i.e. oblique impact testing) of the synthesized oblique FRFs using 115 sets of various impact directions.

From Fig. 6(a), the obtained natural frequencies range from 11.16 Hz to 11.48 Hz depends on the oblique angle set, with an average of  $(11.28 \pm 0.06)$  Hz. The oblique impact testings using various oblique directions only manage to extract one of the coupled modes in Mode #1. This is because the single oblique reference approach fails to identify the coupled mode, especially the dynamically complex mode with multiple mode shapes in various orthogonal planes in this study. Compared to the benchmark results of Mode #1 by y-excitation (i.e. 11.29 Hz) and Mode #1 by z-excitation (i.e. 11.35 Hz), the

highest percentage errors of 1.68% and 1.67% are obtained respectively. Besides, the mean percentage error of  $(0.48 \pm 0.33)\%$  and  $(0.69 \pm 0.48)\%$  are obtained for Mode #1 by y- and z-excitations respectively. From Fig. 6(b), the obtained natural frequencies range from 15.08 Hz to 15.24 Hz for Mode #2, with an average of  $(15.22 \pm 0.03)$  Hz. There are 32 out of 115 oblique directions of synthesized oblique FRFs unable to extract Mode #2. However, the rest shows good agreement of natural frequency estimation. The highest percentage error of 0.98% and mean percentage error of  $(0.07 \pm 0.21)\%$  are obtained, compared to the benchmark results of Mode #2 by y-excitation (i.e. 15.23 Hz). Fig. 6(c) shows that the obtained natural frequencies range from 18.21 Hz to 18.37 Hz for Mode #3, with an average of  $(18.25 \pm 0.02)$  Hz. The highest percentage error of 0.71% and mean percentage error of  $(0.08 \pm 0.13)\%$  are obtained, compared to the benchmark results of Mode #3 by y-excitation (i.e. 18.24 Hz). Overall, the oblique impact testing with single impact reference DOF in current practice only manages to extract 3 out of 4 modes within the frequency range of interest, regardless of impact directions. This demonstrates the drawback of the conventional oblique impact testing that replaces tri-axial normal impacts with a single oblique impact, as one of the coupled modes in Mode #1 is unable to be extracted. In many cases, the user might fail to reveal the intractable mode, without even notice it. Thus, extra care must be taken when oblique impact testing is applied and there is room for improvement to tackle the coupled-mode issue. Furthermore, most of the oblique directions can adequately estimate the natural frequencies for directional modes such as Mode #2 by y-excitation and Mode #3 by z-excitation in this study. However, it is found that the wrong selection of impact directions may lead to failure in estimating some vibration modes. So, a suitable impact direction is crucial to ensure the success of oblique impact testing.

**Fig. 5** 115 sets of impact directions selected for the feasibility study of oblique impact testing.

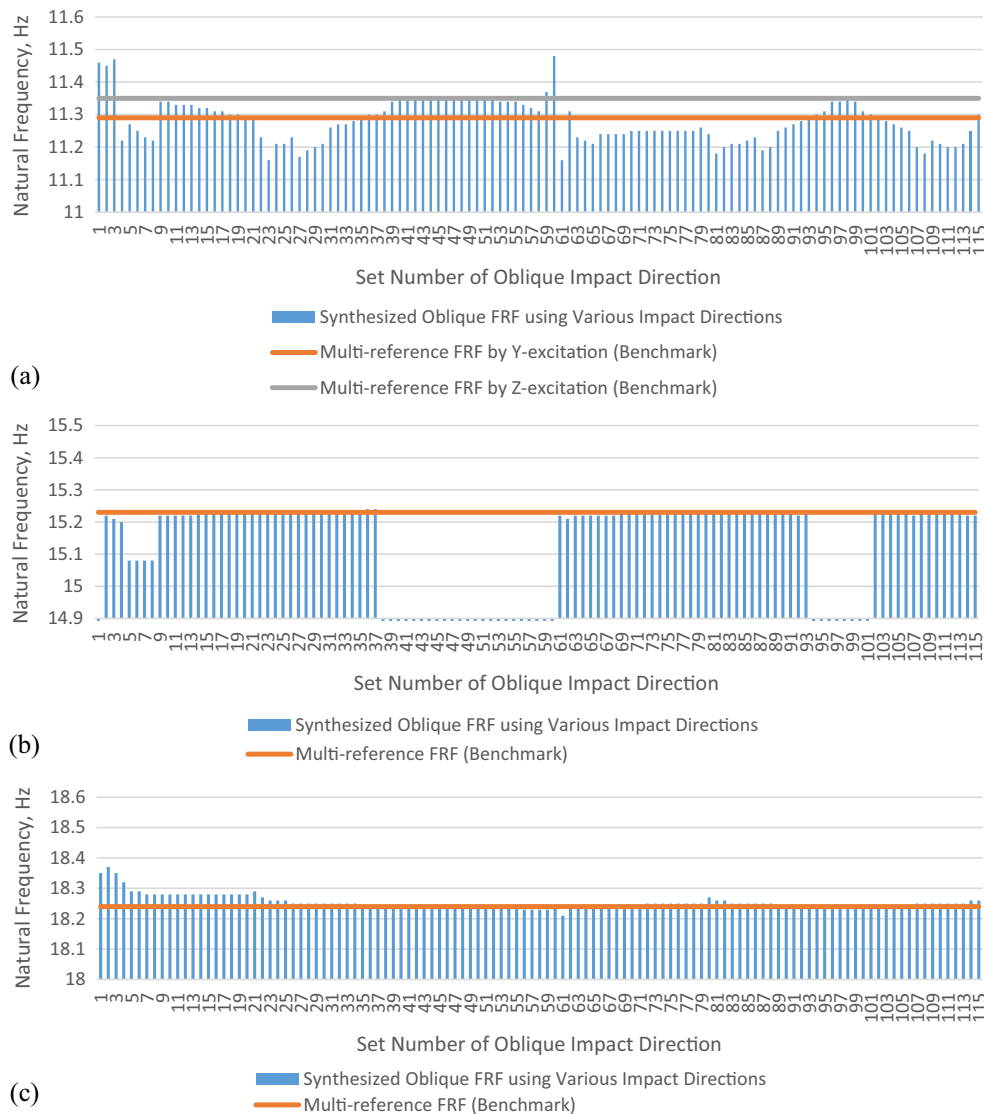


**Fig. 6** Natural frequency estimation of (a) Mode #1, (b) Mode #2, and (c) Mode #3 from the oblique impact testings using various impact directions.

Next, the modal damping ratio results for Modes #1 to #3 are given in Fig. 7. Fig. 7(a) shows that the obtained modal damping ratio ranges from 1.18% to 4.18%, with an average of  $(2.58 \pm 0.62)\%$  for Mode #1. The highest absolute errors of 2.08% and 1.68% are obtained respectively, compared to the benchmark results of Mode #1 by y-excitation (i.e. 2.05%) and Mode #1 by z-excitation (i.e. 2.45%). Besides, the mean absolute error of  $(0.65 \pm 0.49)\%$  and  $(0.46 \pm 0.43)\%$  are obtained for Mode #1 by y- and z-excitations respectively. Next, there are 32 out of 115 oblique angles of synthesized oblique FRF unable to extract Mode #2. However, the rest shows a satisfactory estimation of the modal damping ratio. From Fig. 7(b), the obtained modal damping ratio ranges from 2.60% to 3.80%, with an average of  $(3.68 \pm 0.30)\%$  for Mode #2. The highest absolute error and the mean absolute error of 1.20% and  $(0.12 \pm 0.30)\%$  are obtained respectively, compared to Mode #2 by y-excitation (i.e. 3.80%). For Mode #3, the obtained modal damping ratio ranges from 0.62% to 1.19%, with an average of  $(1.11 \pm 0.12)\%$  as shown in Fig. 7(c). The highest absolute error and

the mean absolute error of 0.54% and  $(0.06 \pm 0.11)\%$  are obtained respectively, compared to the benchmark result of Mode #3 by z-excitation (i.e. 1.16%). Overall, oblique impact testings show a good estimation of modal damping ratio (i.e. mean absolute error less than 0.65% among all modes) in most of the examined impact directions, provided the mode is successfully excited in the selected oblique directions.

The third parameter to be examined is the mode shape. First of all, mode shapes obtained from 60 sets of synthesized oblique FRFs using various 2D oblique excitations are compared to the mode shapes obtained from multi-reference FRF using MAC in Fig. 8.

The color bar shows that high MAC value close to yellow color has an excellent correlation of mode shape, while low MAC value close to blue color has a poor correlation of mode shape. Note that impact direction that causes MAC value greater than or equal to 0.9 is labelled with 'O', and impact directions with 'X' label indicates that the mode is unsuccessfully excited in that particular direction. Lines #1, #2 and #3 are used to represent 2D impact force directions with changing

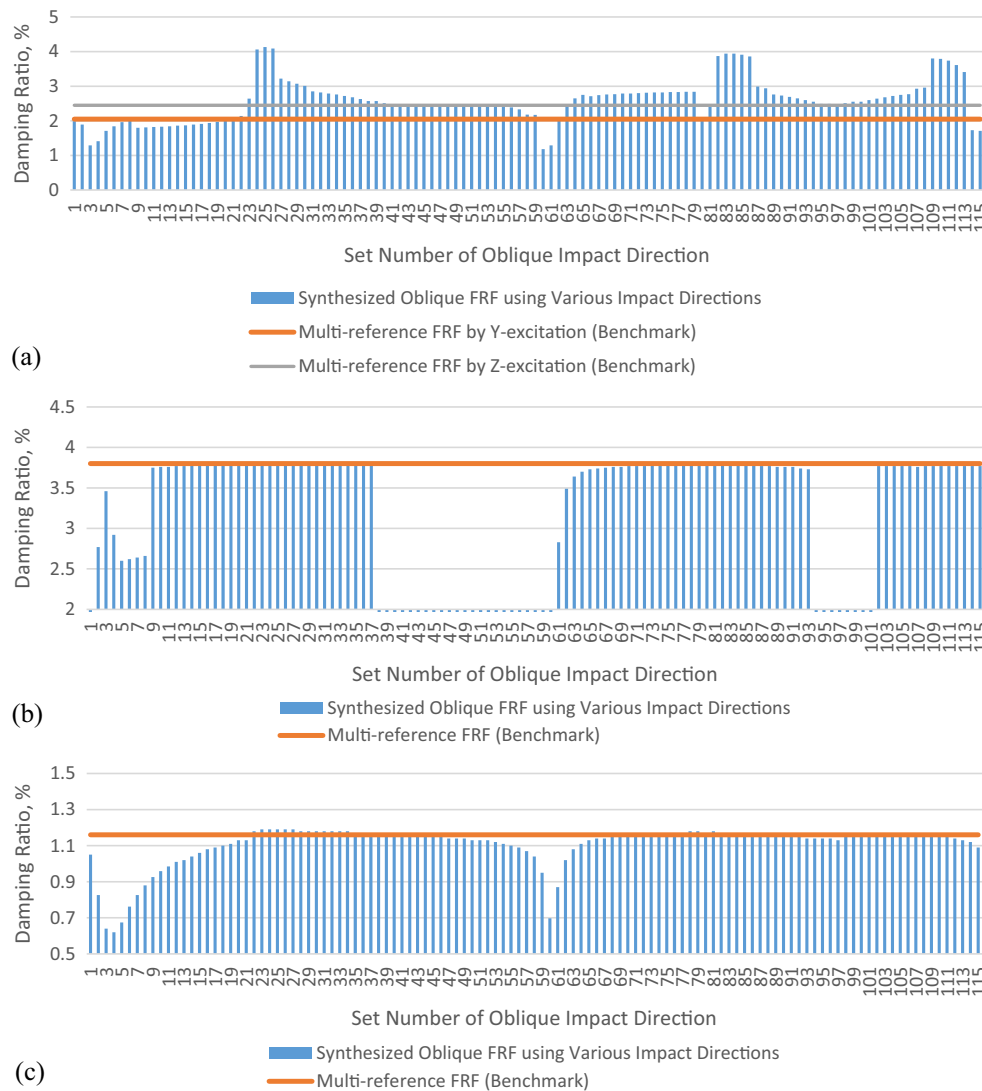


**Fig. 7** Modal damping ratio estimation of (a) Mode #1, (b) Mode #2, and (c) Mode #3 from the oblique impact testings using various impact directions.

force strength in the  $xy$ -,  $yz$ - and  $xz$ - planes respectively. For example, the arrow of Line #1 in Fig. 8 shows the selection of 2D impact directions in the  $xy$ -plane with increasing  $y$ -excitation component or strength while reducing  $x$ -excitation strength, when it is moving towards the  $y$ -axis, and vice-versa. Arrow of Line #2 in Fig. 8 is moving from  $y$ -axis to  $z$ -axis, indicating the impact directions with increasing  $z$ -excitation strength while reducing  $y$ -excitation strength, and vice versa. Arrow of Line #3 in Fig. 8 shows the impact directions with increasing  $x$ -excitation strength while reducing  $z$ -excitation strength, as it is moving from  $z$ -axis to  $x$ -axis.

Mode #1 of the synthesized oblique FRFs obtained from the oblique impact testings using various 2D impact directions is compared to the benchmark results (i.e. coupled modes of Mode #1 by  $y$ -excitation and Mode #1 by  $z$ -excitation) in Fig. 8(a) and (b). Compared to Mode #1 by  $y$ -excitation in Fig. 8(a), the highest MAC values obtained for the 2D forces acting in  $xy$ -,  $yz$ - and  $xz$ -planes (i.e. Lines #1, #2 and #3) are 0.926, 0.909 and 0.739 respectively. Poor MAC values are obtained in Line #3 because the excitation in  $xz$ -plane pro-

duces zero  $y$ -excitation to excite the Mode#1 by  $y$ -excitation. It is observed that MAC values are increasing when Lines #1 and #2 are heading towards the  $y$ -axis. This shows that increasing force strength in  $y$ -component is useful to improve the MAC value of the Mode #1 by  $y$ -excitation. On the other hand, the comparison with Mode #1 by  $z$ -excitation in Fig. 8 (b) shows that the highest MAC values obtained for the 2D forces acting in  $xz$ -,  $yz$ - and  $xy$ -plane (i.e. Lines #3, #2 and #1) are 0.972, 0.984 and 0.538 respectively. Poor MAC values are obtained in Line #1 because the excitation in  $xy$ -plane produces zero  $z$ -excitation, which has poor strength to extract the Mode#1 by  $z$ -excitation. It is observed that MAC values are increasing when Lines #2 and #3 are moving towards the  $z$ -axis. This shows that increasing force strength in  $z$ -component is useful to improve the MAC value of the Mode #1 by  $z$ -excitation.

Comparing Fig. 8(a) and (b) shows that the increasing contribution of  $z$ -component force will reduce the quality of MAC value in Mode #1 by  $y$ -excitation, while the increasing contribution of  $y$ -component force will reduce the quality of MAC

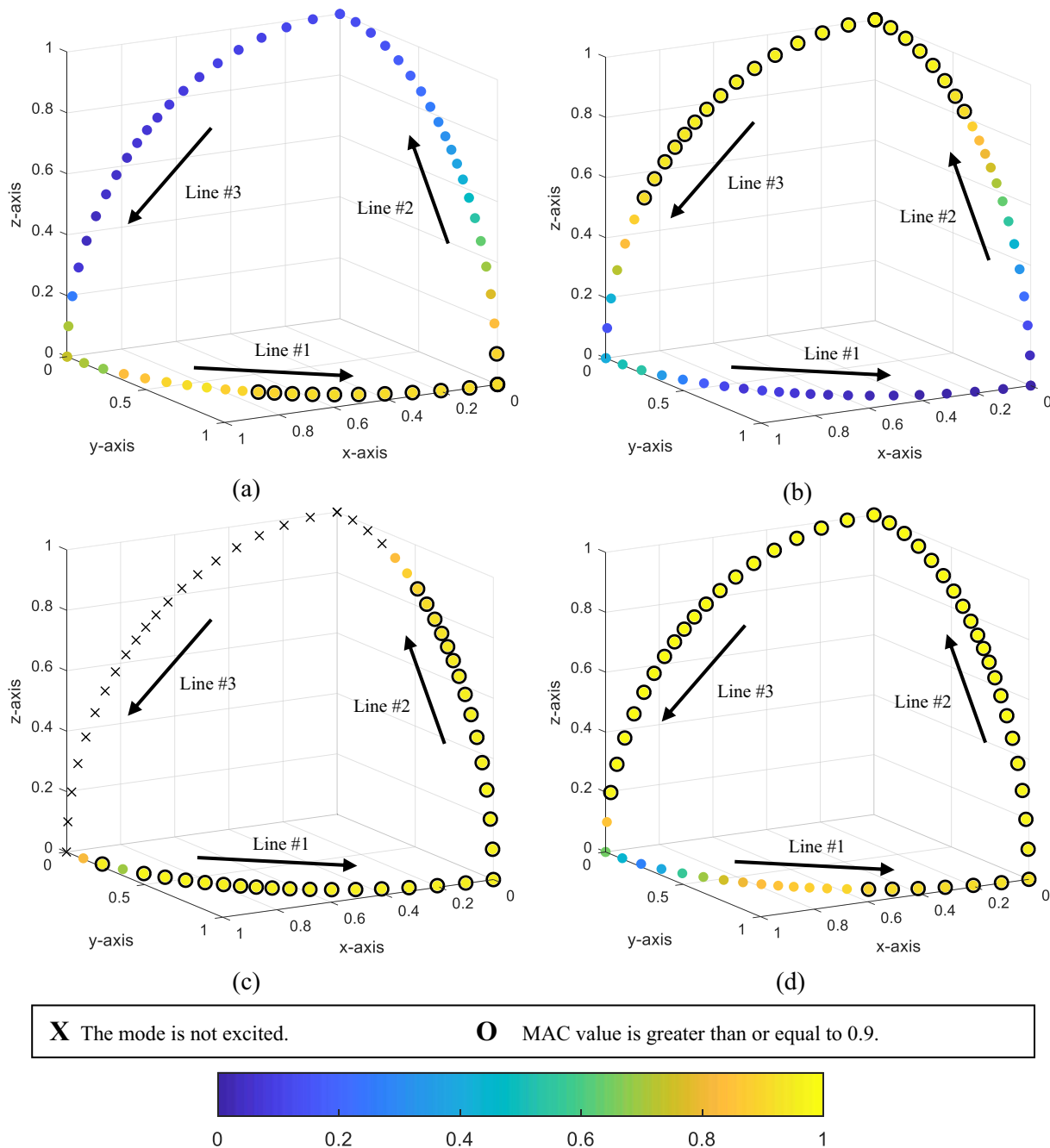


**Fig. 8** MAC comparison of (a) Mode #1 by y-excitation, (b) Mode #1 by z-excitation, (c) Mode #2 by y-excitation, and (d) Mode #3 by z-excitation for 2D oblique excitation.

value in Mode #1 by z-excitation. This can be observed from the results where Line #1 has more successful impact directions with MAC values  $\geq 0.9$  than Line #2 and the highest MAC value obtained from impact directions in Line #1 (i.e. 0.926) is higher than the one in Line #2 (i.e. 0.909), as shown in Fig. 8(a). Close examination of this relationship shows that the oblique impacts near the center of Line #2 will excite both Modes #1 by y- and z-excitations simultaneously, thus it causes modal coupling between the closely coupled modes (or mode shape superposition between orthogonal modes), hence causing poor MAC values in both coupled modes. However, the oblique impacts near the center of Line #1 will excite

mainly the Mode #1 by y-excitation because there is no z-excitation component. For the Mode #1 by z-excitation, Line #3 has more successful impact directions with MAC values  $\geq 0.9$  than Line #2 and the mean MAC value obtained from impact directions in Line #3 (i.e.  $0.85 \pm 0.23$ ) is higher than the one in Line #2 (i.e.  $0.67 \pm 0.34$ ), as shown in Fig. 8(b). This is because oblique impact at the center of Line #2 will excite both coupled modes simultaneously as discussed above, thus the modal coupling effect reduces the obtained MAC value in this impact region. However, the oblique impact at the center of Line #3 will excite mainly Mode #1 by z-excitation because there is no y-excitation component. Thus,

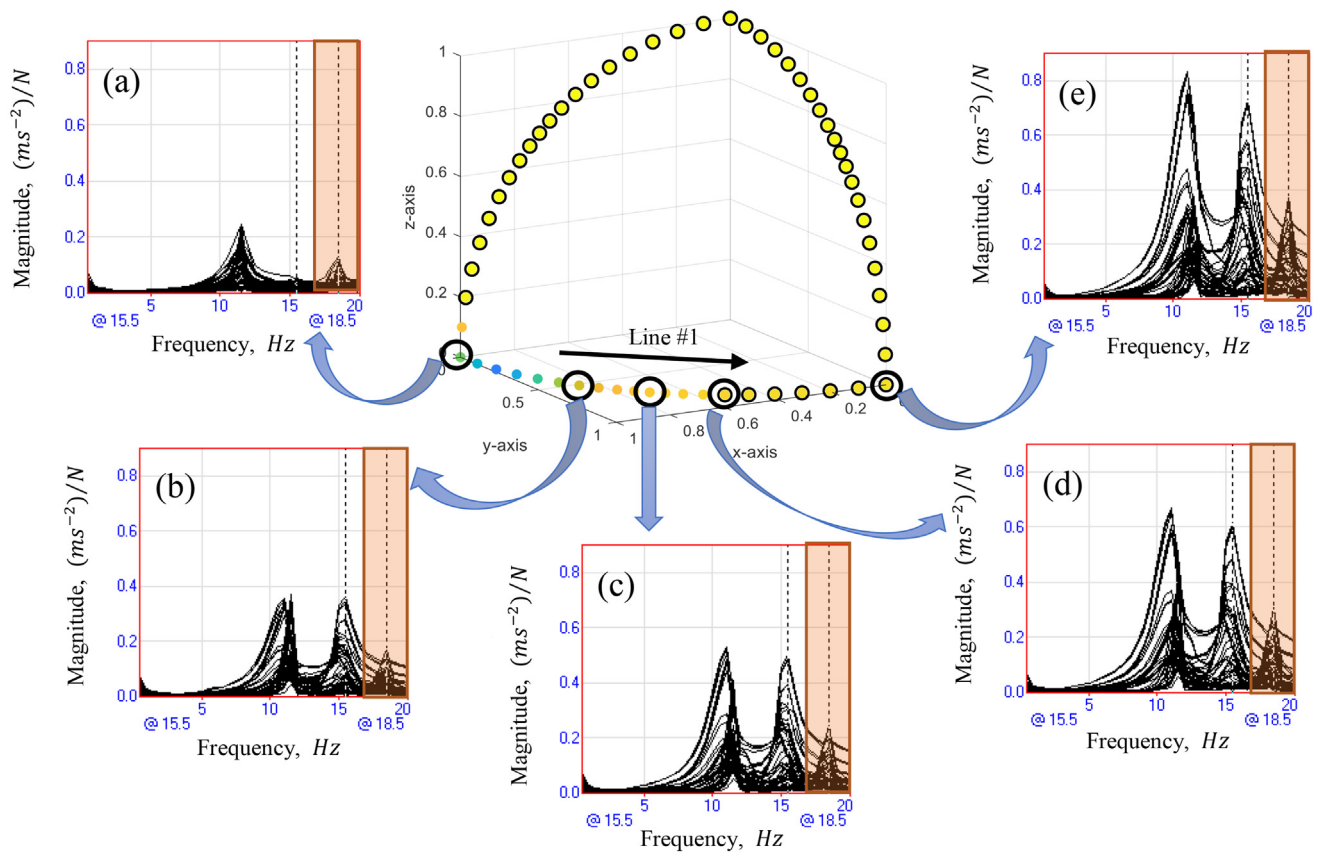


**Fig. 9** Synthesized FRFs due to impact directions of (a)  $\{1, 0, 0\}$ , (b)  $\{0.86, 0.52, 0\}$ , (c)  $\{0.71, 0.71, 0\}$ , (d)  $\{0.52, 0.86, 0\}$ , and (e)  $\{0, 1, 0\}$ .

more impact directions are obtained in Line #3 to obtain high MAC values in Mode #1 by z-excitation because it is not affected by the modal coupling effect.

Mode #2 mode shapes of the synthesized oblique FRFs obtained from the oblique impact testings using various 2D impact directions are compared to the benchmark result (i.e. Mode #2 by y-excitation which has been identified as y-axis dominant mode earlier) in Fig. 8(c). It shows that impacts in the xz-plane (i.e. Line #3) fails to extract the Mode #2, due to the absence of y-excitation component. It is observed that MAC values are increasing when Lines #1 and #2 are heading towards the y-axis with the highest MAC values of 0.972 and 0.970 are obtained respectively in these two lines. This shows the importance of enhancing the y-excitation contribution to ensure a successful mode shape estimation in Mode #2. Moreover, few oblique impact angles in Line #2 that near to z-axis and Line #1 that near to x-axis shows poor MAC values. This is because the low strength y-excitation in impact directions far away from the y-axis is inadequately to excite the Mode #2, hence causing poor extraction of the mode shape.

In Fig. 8(d), Mode #3 mode shape of synthesized oblique FRFs obtained from the oblique impact testings using various 2D impact directions are compared to the benchmark result (i.e. Mode #3 by z-excitation which has been identified as z-axis dominant mode earlier). It is observed that MAC values are increasing when Lines #2 and #3 are heading towards the z-axis with the highest MAC values of 0.994 and 0.994 are obtained respectively in these two lines. This shows the

importance of enhancing the z-excitation contribution to extract Mode #2 mode shape successfully. Theoretically, low strength z-excitation in impact directions far away from the z-axis will cause the poor extraction of the mode shape. It is surprising to see the impact directions in Line #1 with zero z-excitation can excite the Mode #3 mode shape with high accuracy. To further examine the issue, the obtained synthesized FRFs using impact directions in Line #1 are compared in Fig. 9. It is observed that the global peak of FRF in Mode #3 (highlighted in orange color) is increasing when the oblique impact is moving towards the y-axis. This indicates that the modal strength of the Mode #3 increases with the increment strength of the y-excitation which ensures the success of the mode shape estimation in this impact region. So, the modal strength of FRF plays an important role to excite a particular vibration mode besides the force strength.

Comparing Fig. 8(c) and (d) shows that oblique impacts in 2D directions in the yz-planes (i.e. Line #2) especially the middle region can adequately excite both directional modes Modes #2 and #3. However, careful examination of Fig. 8(a)–(d) show that no single 2D impact direction can sufficiently excite all 4 modes in this study. Commonly, the oblique angle at  $45^\circ$  to all axes is prominently applied in the previous study [5,21,22]. It was assumed that this impact direction can adequately excite all modes of interest. However, it is revealed that this approach imposes a significant drawback, where it poses difficulty especially in extracting all the coupled modes. In the worst-case scenario, the user might estimate the wrong mode shape of

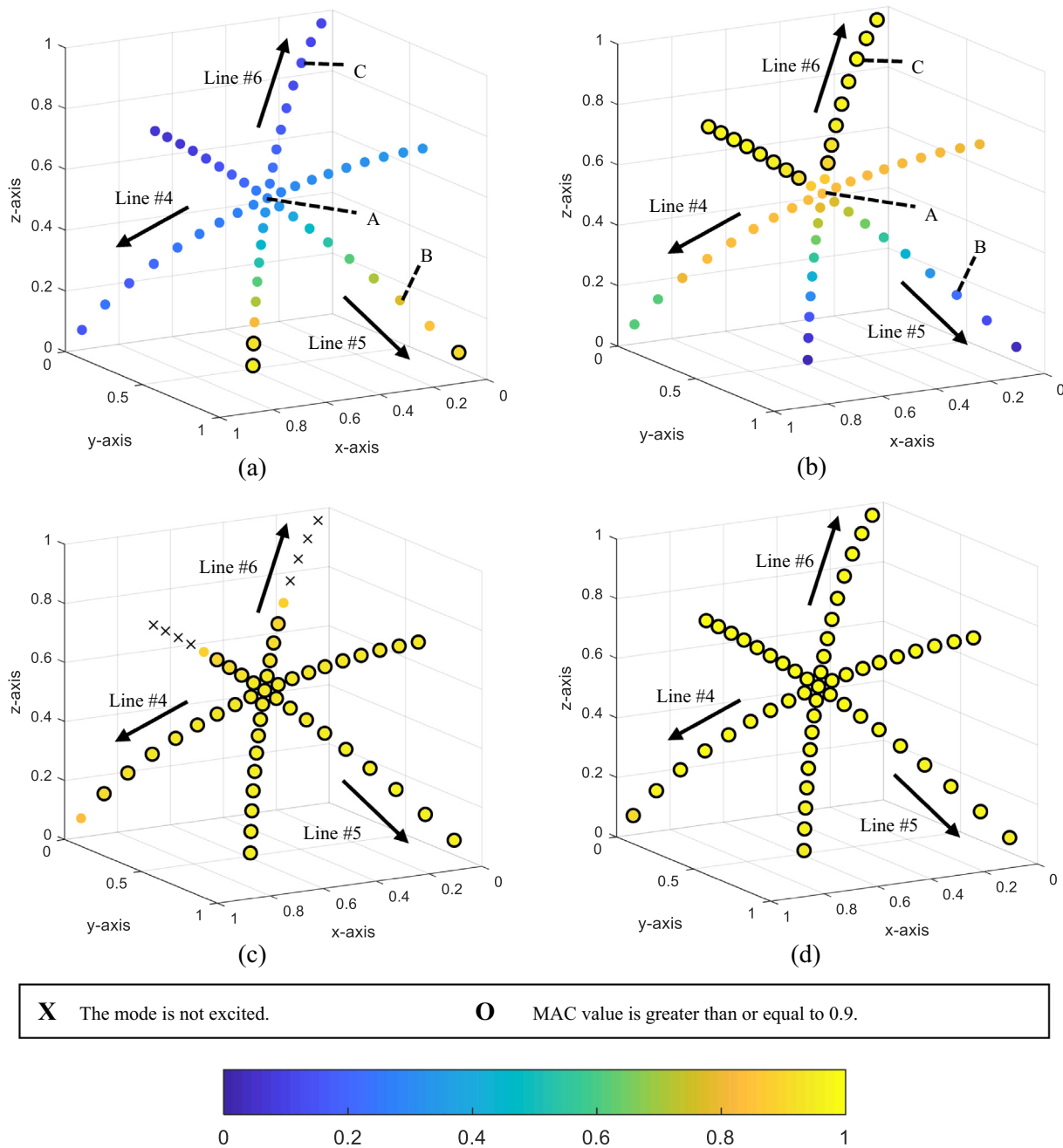


**Fig. 10** MAC comparison of (a) Mode #1 by y-excitation, (b) Mode #1 by z-excitation, (c) Mode #2 by y-excitation, and (d) Mode #3 by z-excitation for 3D oblique excitation.

Mode #1, which is suffered from the modal coupling effect, without even notice it. This problem shows the deficiency of the current practice in implementing the oblique impact testing with the invalid assumption that it can estimate all modes in various orthogonal planes without concerning the impact directions. It is important to aware that the selection of a proper impact direction is crucial to ensure good estimations of all modal parameters.

Next, mode shapes obtained from 55 sets of synthesized oblique FRFs using various 3D oblique excitations are compared to the mode shapes obtained from multi-reference FRF using MAC in Fig. 10. Lines #4, #5 and #6 are used to represent 3D impact directions with changing force strength

in the xyz- plane. For example, the arrow of Line #4 in Fig. 10 shows the selections of 3D impact directions moving towards x-axis have increasing x-excitation component or strength while reducing both the y- and z- excitations strength. Note that both y- and z- excitations strengths are equal so that the effect of the changing x-excitation can be investigated. Arrows of Lines #5 and #6 are moving towards y- and z- axes respectively as shown in Fig. 10. The selections of impact directions in these lines are having increasing y- and z- excitations components respectively, while the strengths of other excitations in the other two directions are reducing. Note that these excitations in other directions have equal strength so that the effect of changing y- and z- excitations can be investigated

properly. It is worthwhile to mention that the mid-intersection point of Lines #4 to #6 has the equivalent force strength in 3 principal directions.

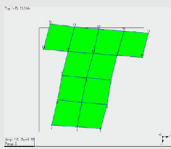
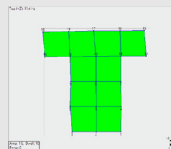
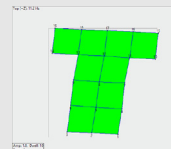
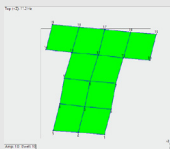
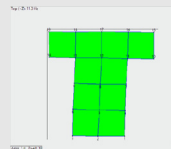
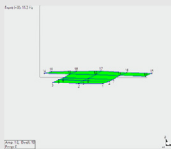
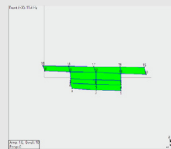
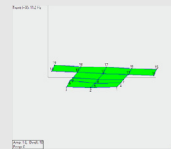
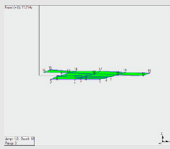
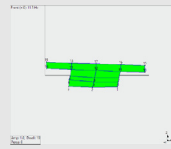
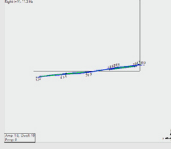
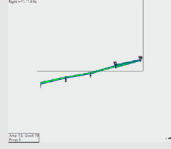
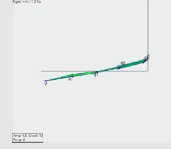
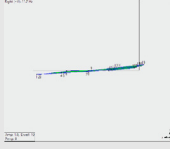
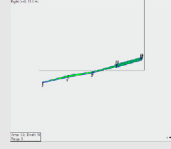
Mode #1 of synthesized oblique FRF obtained from the oblique impact testings using various 3D impact directions is compared to the benchmark results (i.e. coupled mode of Mode #1 by y-excitation and Mode #1 by z-excitation) in Fig. 10(a) and (b). Compared to Mode #1 by y- excitation in Fig. 10(a), the highest MAC values obtained in Lines #6, #5 and #4 are 0.968, 0.913, and 0.340 respectively. Compared to Mode #1 by z- excitation in Fig. 10(b), the highest MAC values obtained in Lines #5, #6 and #4 are 0.992, 0.987, and 0.843 respectively. Comparing both Fig. 10(a) and (b), it was found that impact region in Line #4 is not favourable because it has the lowest MAC values (MAC < 0.35). This is because the changing x-excitation strength does not affect the quality of the Mode #1 by y-excitation. At the same time, both strengths of y- and z- excitations are increasing at the same rate when it moves away from the x-axis, which will excite both Mode #1 by y- and z- excitations simultaneously. In other words, y- and z-excitations have an equal force strength in Line #4. This causes the modal coupling problem that reduces the MAC quality for both coupled modes in this impact region, as discussed previously. In addition, impact region in Lines #5 and #6 produces excellent MAC values (labelled by ‘O’ in Fig. 10 (a)) in Mode #1 by y-excitation when the impacts move towards the y-axis and away from the z-axis respectively. Both lines experience increasing strengths in y-excitation which provides sufficient excitation to extract Mode #1 by x-excitation. Line #6 has greater MAC value than Line #5, this is because the z-excitation strength is reduced at a higher rate in Line

#6 compared to Line #5. This ensures that the modal coupling effect can be minimized to a negligible stage for enhancing the modal parameter extraction. In contrast, when the impact moves away from the y-axis and towards the z-axis for the Lines #5 and #6 respectively, excellent MAC value of the Mode #1 by z-excitation can be obtained as shown in Fig. 10(b). This is due to the increasing z-excitation strength for the extraction of the second coupled mode. In this case, Line #5 has greater MAC value than Line #6 because y-excitation strength is reduced at a higher rate, which leads to higher reduction of the modal coupling effect.

To further illustrate the modal coupling effect in the extraction of couple modes using various impact directions, 3 cases are studied by using impact directions of A, B, and C, as shown in Fig. 10(a) and (b), and the results are reported in Table 6. Case A in Table 6 shows that the modal coupling effect will occur if the selected impact direction (e.g. impact A) excites all coupled modes simultaneously, which causes the mode shape superposition of the coupled modes. The modal coupling effect can be reduced to a satisfactory level if one of the coupled modes is predominantly excited per impact (e.g. impact B predominantly excites the Mode #1 by y-excitation or impact C predominantly excites the Mode #1 by z-excitation). This point is further confirmed in Cases B and C when the obtained mode shapes in the selected impact directions (i.e. impacts B and C) are similar to both coupled modes obtained from the benchmark study, as shown in Table 6.

Compared to the coupled modes, the directional modes such as Mode #2 by y-excitation (i.e. y-dominant mode shape) or Mode #3 by z-excitation (i.e. z-dominant mode shape) can

**Table 6** Mode #1 coupled modes excited by using various impact directions.

Case	Benchmark Study		Synthesized Oblique FRF Using Various Impact Directions		
	Case I (Mode #1 by y- excitation)	Case II (Mode #1 by z- excitation)	Case A (Equal force strength in 3D directions)	Case B (High force strength in y-directions)	Case C (High force strength in z-directions)
Characteristic	Yaw & Pitch Motions	Surge & Pitch Motions	Yaw, Surge & Pitch Motions	Yaw & Pitch Motions	Surge & Pitch Motions
Top View					
Front View					
SideView					
Observation	Dominant in y- direction	Dominant in z- direction	Dominant in y- and z- directions	Dominant in y-direction	Dominant in z-direction
Analysis	Coupled Mode I	Coupled Mode II	Modal Coupling/Mode Shape Superposition	Similar to Coupled Mode I	Similar to Coupled Mode II

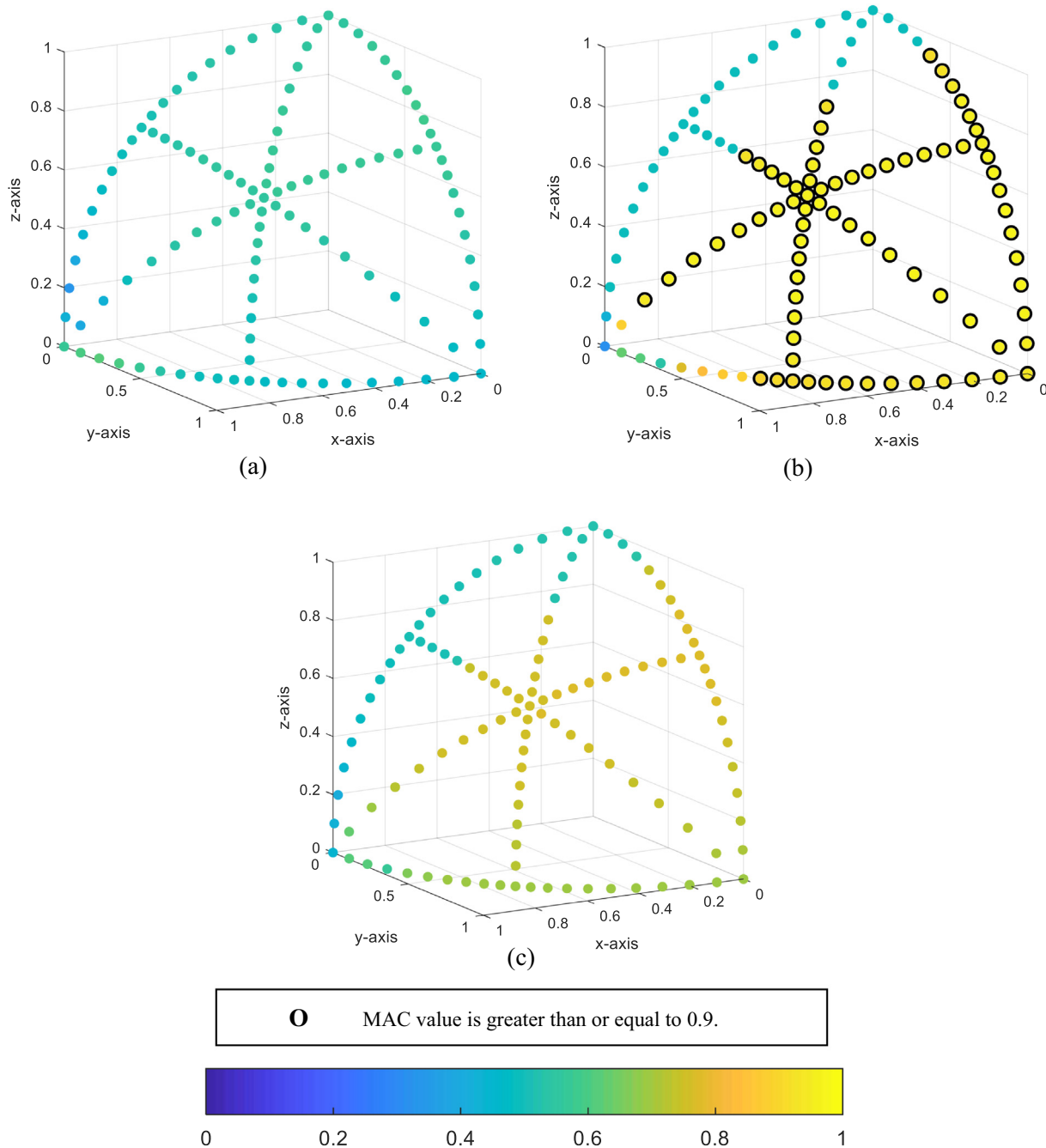


**Fig. 11** Mean MAC value of (a) Mode #1 by y-excitation and Mode #1 by z-excitation, (b) Mode #2 by y-excitation and Mode #3 by z-excitation, and (c) all mode shapes.

be easily excited using 3D oblique impact. This is because 3D oblique impacts impose force strength in all principal directions and it is expected that it can adequately excite all the directional modes in different orthogonal planes. In this study, the highest MAC values of Mode #2 obtained in Lines #1 to #3 are 0.944, 0.969, and 0.968 respectively. Similar to the 2D impact case, y-excitation strength plays an important role to excite Mode #2. Fig. 10(c) shows that insufficient y-excitation strength at the upper part (i.e. furthest side from y-axis) causes unsuccessful mode extraction and vice versa. For Mode #3, the highest MAC values obtained in Lines #1 to #3 are 0.992, 0.994, and 0.994 respectively. Fig. 10(d)

demonstrates excellent mode shape estimation (i.e.  $\text{MAC} \geq 0.9$ ) for all the examined oblique directions. It is mainly due to the good contribution of the force and modal strengths, as discussed previously in Figs. 8(d) and 9.

Next, the mean MAC values are examined among the vibration modes, as shown in Fig. 11. Firstly, the mean MAC values of the Mode #1 coupled modes are shown in Fig. 11(a). The mean MAC values of  $(0.54 \pm 0.04)$  and  $(0.52 \pm 0.05)$  are obtained for 3D and 2D impact directions respectively, which validate that 3D excitation has better mode extraction than 2D excitation in this case. It shows that there is no single oblique impact direction that can excite both coupled

modes in Mode #1 simultaneously if a single reference approach is used. If the multi-reference approach is allowable, two oblique references close to y- and z- axes are needed to excite the coupled modes adequately for high MAC value, as illustrated previously in Figs. 8(a) & (b) and 10(a) & (b). In addition, directional modes are much easier to be excited compared to the coupled modes. Fig. 11(b) shows that plenty impact directions that can excite both Modes #2 and #3 simultaneously, where the mean MAC values of  $(0.90 \pm 0.17)$  and  $(0.74 \pm 0.22)$  are obtained for 3D and 2D impact directions respectively. This validates that 3D excitation has better mode extraction than 2D excitation for the case of directional mode. It is important to aware that wrong selection of the oblique angle would result in mode estimation failure for directional mode, as illustrated previously in Figs. 8(c) and 10(c). Fig. 11(c) records the average of all modes obtained in this study. It shows the mean MAC values of  $(0.72 \pm 0.09)$  and  $(0.63 \pm 0.12)$  for 3D and 2D impact directions respectively. It is found that the mean MAC value for all modes can be enhanced to  $(0.76 \pm 0.01)$  if the 3D oblique impact region is selected about  $\pm 15^\circ$  from the mid-intersection impact direction. This shows that oblique impact is unnecessarily limited to the equally distributed force strength in the mid-intersection impact direction, to achieve high MAC results. Moreover, the user can consider performing the oblique impact testing in mid-section of 2D yz-plane for similar T-shaped test rig as it produces high MAC value within these impact regions.

The selection of oblique impact in 2D directions are having much lower accuracy in extracting the mode shapes especially if the vibration modes of the examined structure are unknown in a priori. This situation can be improved by implementing theoretical modelling or simulation technique for the pretest analysis, so that proper planning such as the suitable impact direction can be studied in advanced of the experimental work. To a large extent, the oblique impact testing with single impact direction applied in the current practice has a good ability to extract directional modes. However, it poses obstacle in obtaining the complete set of coupled modes due to the modal coupling effect. This demonstrates the limitation of the current practice and thus the practicality of the existing oblique impact testing should be further enhanced in the future work.

#### 4. Conclusion

In this study, a synthesis method to generate oblique FRF due to any impact directions has been successfully developed. The validation of the synthesis oblique FRF method gives reliable results, as high accuracy of FRF and modal parameter results are obtained, as compared with the benchmark study (i.e. EMA with tri-axial normal impact testing). The results show good mean oblique FRF correlations of  $(0.96 \pm 0.02)$ , low mean percentage error  $(0.40 \pm 0.28)\%$  of the natural frequency estimations, low mean absolute error  $(0.35 \pm 0.37)\%$  of the modal damping ratio estimations, as well as high mean MAC value  $(0.97 \pm 0.01)$  of mode shape identifications. The proposed synthesis method provides an alternative solution to determine multiples oblique FRFs in many impact directions for the feasibility study. This study has successfully investigated the effect of using various impact directions on the EMA with oblique impact testing, including 2D and 3D

oblique impact directions within an octant. The drawback of the current EMA practice that replaces tri-axial normal impacts with a single oblique impact is highlighted. The result shows that the oblique impact testing using single impact direction can successfully identify all the directional modes in various orthogonal planes (i.e. Modes #2 and #3), however it only manages to identify one of the closely-coupled modes (i.e. it can be either Mode #1 by x-excitation, Mode #2 by y-excitation or the modal coupling between the coupled modes depending on the selected impact direction). In spite of the couple mode issue, the oblique impact testing still can determine accurate natural frequency and modal damping ratio results, by using many impact directions. This is validated by the low mean percentage error of  $(0.07\text{--}0.69)\%$  and low mean absolute error of  $(0.06\text{--}0.65)\%$  obtained for all the examined modes. Furthermore, 3D impact directions have a better mode extraction ability than 2D excitation due to its better force strength in all principal directions. The mean MAC values of  $(0.54 \pm 0.04)$  and  $(0.90 \pm 0.17)$  are obtained for the coupled modes and directional modes respectively by using 3D impact directions. It is found that directional modes can be excited adequately if the selected impact direction has a good contribution in terms of force and modal strengths. Poor MAC values obtained for the coupled modes are mainly due to the modal coupling effect, as illustrated and explained in this study. It is urged that the existing oblique impact testing with a single impact direction should be enhanced further in future work to tackle this issue. In all, selection of proper impact direction in oblique impact testing is an important criterion and it should not be neglected to ensure an accurate estimation of structural dynamic characteristics.

#### Declaration of Competing Interest

The authors declare that they have no known competing financial interests or personal relationships that could have appeared to influence the work reported in this paper.

#### Acknowledgement

The authors wish to acknowledge the financial support given by the Fundamental Research Grant Scheme (FP057-2015A) and the advice given by Advanced Shock and Vibration Research (ASVR) Group of University of Malaya and other project collaborators.

#### References

- [1] P. Avitabile, *Experimental modal analysis - a simple non-mathematical presentation*, *Sound Vib.* 35 (1) (2001) 20–31.
- [2] M. Elshamy, W.A. Crosby, M. Elhadary, *Crack detection of cantilever beam by natural frequency tracking using experimental and finite element analysis*, *Alex. Eng. J.* 57 (2018) 3755–3766.
- [3] A. Eraky, A.M. Anwar, A. Saad, A. Abdo, *Damage detection of flexural structural systems using damage index method – experimental approach*, *Alex. Eng. J.* 54 (2015) 497–507.
- [4] A. Abd\_Elsalam, M.A. Gohary, H.A. El-Gamal, *Modal analysis on tire with respect to different parameters*, *Alex. Eng. J.* 56 (2017) 345–357.
- [5] O. Dossing, *Improvement to monoreference modal data by adding an oblique degree of freedom for the reference*, in:

- Proceedings of the 4th International Modal Analysis Conference (IMAC IV), Los Angeles Airport Marriott Hotel, Los Angeles, CA, 2001, pp. 1175–1180.
- [6] N.H. Baharin, R.A. Rahman, Effect of accelerometer mass on thin plate vibration, *J. Mekanikal.* 29 (2) (2009) 100–111.
- [7] W.A. Fladung, The development and implementation of multiple reference impact testing Master of Science Master's thesis, Department of Mechanical Engineering, University of Cincinnati, Ohio, United States, 1994.
- [8] P. Avitabile, Modal space – Back to basics: Could I use an oblique angle instead?, *Exp Tech.* 24 (3) (2000) 13–14.
- [9] O. Dossing, Multi-reference impact testing for modal analysis using type 3557 fourchannel analyzer and CADA-PC, Denmark, 1994.
- [10] P. Avitabile, Modal space - Back to basics: Is there any benefit to using multiple references?, *Exp. Techniques.* 25 (4) (2001) 19–20.
- [11] I. Vibrant Technology, Multi-reference Curve Fitting to Find Repeated Roots, USA, 2019.
- [12] H. Herlufsen, Modal Analysis using Multi-reference and Multiple-input Multiple-output Techniques, Denmark, 2004.
- [13] Y.J. Liao, Y. Zhou, P. Qin, Multiple reference impact testing for bridge assessment with drop hammer, *Adv Mater Res.* 605–607 (2013) 718–723.
- [14] I. Vibrant Technology, Multiple Reference Curve Fitting to Find Closely Coupled Modes, USA, 2019.
- [15] R. Hunady, M. Hagara, Experimental investigation of mode shapes of symmetric structures, *Acta Mechanica Slovaca* 19 (3) (2015) 12–17.
- [16] B. Schwarz, P. McHargue, M. Richardson, Rapid impact™ testing of any size structure, in: Machinery Failure Prevention Technology (MFPT) Conference, Philadelphia, PA, 2019, pp. 1–10.
- [17] S.Y. Khoo, Y.C. Lian, Z.C. Ong, Z. Ismail, S. Noroozi, Time effective structural frequency response testing with oblique impact, *Int. J. Aerosp. Mech. Eng.* 12 (6) (2018) 645–649.
- [18] Y.C. Lian, S.Y. Khoo, Z.C. Ong, Z. Ismail, W.T. Chong, S. Noroozi, Investigation of oblique impulse in experimental modal analysis via finite element method, *Int. J. Mech. Prod. Eng.* 7 (1) (2019) 38–42.
- [19] S.M. Leonard, Increasing the reliability of reciprocating compressors on hydrogen services, *Hydrocarb. Process.* 75 (1) (1996) 67–74.
- [20] T. Knechten, P.J. Van Der Linden, M.-C. Morariu, Improved FRF acquisition method for vehicle body NVH analysis, *Sound Vib.* 51 (4) (2017) 8–13.
- [21] C. Warren, C. Niezrecki, P. Avitabile, FRF measurements and mode shapes determined using image-based 3D point-tracking, in: Modal Analysis Topics, Volume 3, Conference Proceedings of the Society for Experimental Mechanics Series, New York, 2011, pp. 243–252.
- [22] C. Warren, C. Niezrecki, P. Avitabile, P. Pingle, Comparison of FRF measurements and mode shapes determined using optically image based, laser, and accelerometer measurements, *Mech. Syst. Signal Process.* 25 (6) (2011) 2191–2202.
- [23] P. Avitabile, Modal space - Back to basics : If I run a shaker test with the input oblique to the global coordinate system, how do I decompose the force into the specific components in each direction?, *Exp Tech.* 33 (5) (2009) 11–12.
- [24] J. Baqersad, P. Poozesh, C. Niezrecki, P. Avitabile, Comparison of modal parameters extracted using MIMO, SIMO, and impact hammer tests on a three-bladed wind turbine, in: Topics in Modal Analysis II, Volume 8, Conference Proceedings of the Society for Experimental Mechanics Series, 2014, pp. 185–197.
- [25] S.E. Obando, J. Baqersad, P. Avitabile, Improved modal characterization using hybrid data, *Sound Vib.* 48 (6) (2014) 8–12.
- [26] M. Luczak, A. Vecchio, B. Peeters, L. Gielen, H. Van der Auweraer, Uncertain parameter numerical model updating according to variable modal test data in application of large composite fuselage panel, *Shock Vib.* 17 (4–5) (2010) 445–459.
- [27] K. Anderson, NuMI/NOvA 700kW horn 1 stripline vibration measurements, 9th International Workshop on Neutrino Beams and Instrumentation (NBI), Fermi National Accelerator Laboratory, Batavia, United States, 2014.
- [28] K. Patil, J. Baqersad, J. Bastiaan, Effects of boundary conditions and inflation pressure on the natural frequencies and 3D mode shapes of a tire, SAE Noise and Vibration Conference and Exhibition Grand Rapids, MI, United States, 2017.
- [29] T. Knechten, M.-C. Morariu, P. van der Linden, Improved method for FRF acquisition for vehicle body NVH analysis, in: SAE Noise and Vibration Conference and Exhibition Grand Rapids, MI, United States, 2015, pp. 1–8.
- [30] L. Verdenelli, R. Rossetti, P. Chiariotti, M. Martarelli, L. Scalise, Experimental and numerical dynamic characterization of a human tibia, *J. Phys. Conf. Ser.* 1149 (1) (2018) 012029.
- [31] ISO, ISO 7626-1:2011(E), Mechanical Vibration and Shock – Experimental Determination of Mechanical Mobility – Part 1: Basic Terms and Definitions, and Transducer Specifications, 2011.
- [32] J. Dimitrijevic, Complex mode indicator function to find repeated roots or closely coupled modes, *Sci.-Tech. Rev.* 55 (3–4) (2005) 50–58.
- [33] R. Allemang, D. Brown, A complete review of the complex mode indicator function (CMIF) with applications, in: Proceedings of ISMA International Conference on Noise and Vibration Engineering, Katholieke Universiteit Leuven, Belgium, 2006, pp. 3209–3246.
- [34] A.R. Barrett, Dynamic testing of in-situ composite floors and evaluation of vibration serviceability using the finite element method Doctoral thesis, Department of Civil Engineering, Virginia Polytechnic Institute and State University, Blacksburg, VA, 2006.
- [35] B. Schwarz, M. Richardson, Post-processing ambient and forced response bridge data to obtain modal parameters, in: Proceedings of IMAC-XIX: A Conference on Structural Dynamics, Hyatt Orlando, Kissimmee, Florida, 2001, pp. 829–835.
- [36] M. Richardson, B. Schwarz, Modal parameter estimation from operating data, *Sound Vib.* 37 (1) (2003) 28–39.